GRAVITATIONAL LENSING

11 - MICROLENSING IV : MULTIPLY IMAGED QUASARS

R. Benton Metcalf

2022-2023

MICROLENSING OF MULTIPLY IMAGED QSOs

Distant quasars can be gravitationally lensed into multiple (two or four) resolved images.

The light path for each of these images may be microlensed by stars in the lens galaxy.

This can be detected by independent variations in the light curve of the images once the time-delay between them have been subtracted.

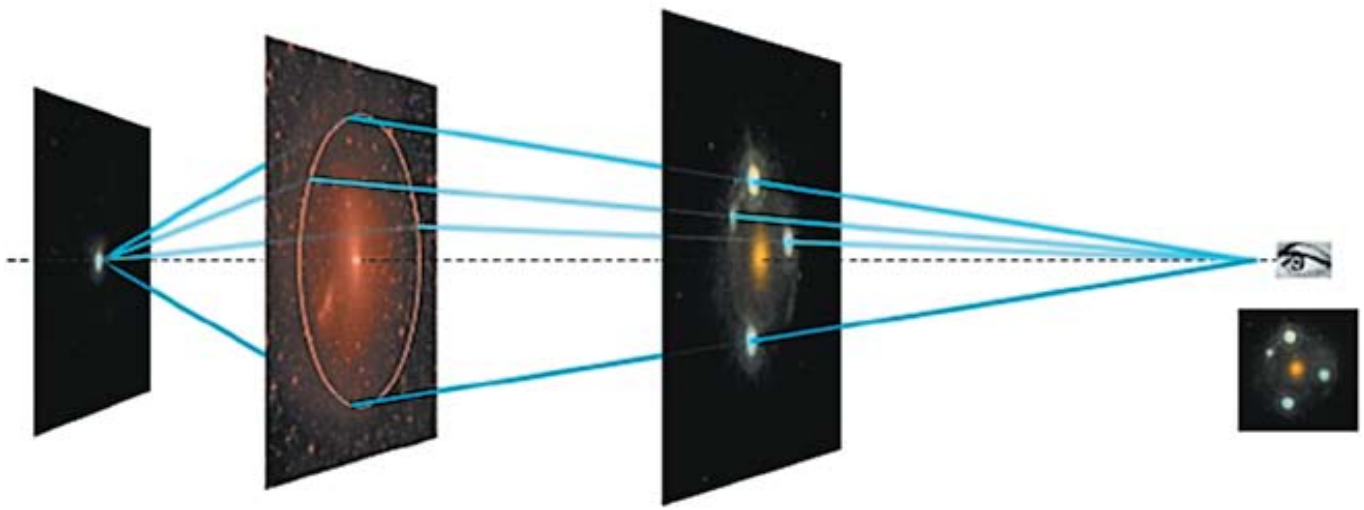

COSMOLOGICAL DISTANCES

coordinate distance

$$\chi(z_s) = \frac{c}{H_o} \int_0^{z_s} \frac{dz}{\sqrt{\Omega_m (1+z)^3 + \Omega_\Lambda + (1 - \Omega_m - \Omega_\Lambda)(1+z)^2}}$$

critical density

$$\Omega_m = \frac{\rho}{\rho_{\rm crit}} \qquad \rho_{\rm crit} = \frac{3H_o^2}{8\pi G}$$

H_o Hubble parameter

comoving angular size distance

$$D_{CA}(z) = \begin{cases} R_{\rm curv} \sin\left(\frac{\chi}{R_{\rm curv}}\right) & \Omega_m + \Omega_\Lambda < 1 \\ \chi & \Omega_m + \Omega_\Lambda = 1 \\ R_{\rm curv} \sinh\left(\frac{\chi}{R_{\rm curv}}\right) & \Omega_m + \Omega_\Lambda > 1 \end{cases}$$

curvature distance

$$R_{\rm curv} = \frac{c}{H_o\sqrt{1 - \Omega_m - \Omega_\Lambda}}$$

COSMOLOGICAL DISTANCES

coordinate distance

$$\chi(z_s) = \frac{c}{H_o} \int_0^{z_s} \frac{dz}{\sqrt{\Omega_m (1+z)^3 + \Omega_\Lambda + (1 - \Omega_m - \Omega_\Lambda)(1+z)^2}}$$

critical density

$$\Omega_m = \frac{\rho}{\rho_{\rm crit}} \qquad \rho_{\rm crit} = \frac{3H_o^2}{8\pi G}$$

H_o Hubble parameter

comoving angular size distance

$$D_{CA}(z_1, z_2) = \begin{cases} R_{\rm curv} \sin\left(\frac{\chi_1 - \chi_2}{R_{\rm curv}}\right) & \Omega_m + \Omega_\Lambda < 1 \\ \chi_1 - \chi_2 & \Omega_m + \Omega_\Lambda = 1 \\ R_{\rm curv} \sinh\left(\frac{\chi_1 - \chi_2}{R_{\rm curv}}\right) & \Omega_m + \Omega_\Lambda > 1 \end{cases}$$

curvature distance

$$R_{\rm curv} = \frac{c}{H_o \sqrt{1 - \Omega_m - \Omega_\Lambda}}$$

COSMOLOGICAL DISTANCES

coordinate distance

$$\chi(z_s) = \frac{c}{H_o}\int_0^{z_s} \frac{dz}{\sqrt{\Omega_m(1+z)^3 + \Omega_\Lambda + (1-\Omega_m-\Omega_\Lambda)(1+z)^2}}$$

comoving angular size distance

$$D_{CA}(z_1, z_2) = \begin{cases} R_{\rm curv}\sin\left(\frac{\chi_1-\chi_2}{R_{\rm curv}}\right) & \Omega_m + \Omega_\Lambda < 1 \\ \chi_1 - \chi_2 & \Omega_m + \Omega_\Lambda = 1 \\ R_{\rm curv}\sinh\left(\frac{\chi_1-\chi_2}{R_{\rm curv}}\right) & \Omega_m + \Omega_\Lambda > 1 \end{cases}$$

curvature distance

$$R_{\rm curv} = \frac{c}{H_o\sqrt{1-\Omega_m-\Omega_\Lambda}}$$

(proper) angular size distance

$$D_A(z, z_o) = \frac{D_{CA}(z, z_o)}{(1+z)}$$

luminosity distance

$$D_L(z) = (1+z)D_{CA}(z)$$

COSMOLOGICAL DISTANCES

coordinate distance

$$\chi(z_s) = \frac{c}{H_o}\int_0^{z_s} \frac{dz}{\sqrt{\Omega_m(1+z)^3 + \Omega_\Lambda + (1-\Omega_m-\Omega_\Lambda)(1+z)^2}}$$

angular size distance

$$D_A(z_1,z_2) = \frac{1}{1+z_1}\begin{cases} R_{\rm curv}\sin\left(\frac{\chi_1-\chi_2}{R_{\rm curv}}\right) & \Omega_m+\Omega_\Lambda<1 \\ \chi_1-\chi_2 & \Omega_m+\Omega_\Lambda=1 \\ R_{\rm curv}\sinh\left(\frac{\chi_1-\chi_2}{R_{\rm curv}}\right) & \Omega_m+\Omega_\Lambda>1 \end{cases}$$

$z_1 > z_2$

curvature distance

$$R_{\rm curv} = \frac{c}{H_o\sqrt{1-\Omega_m-\Omega_\Lambda}}$$

$$D_{ls} \neq D_s - D_l$$

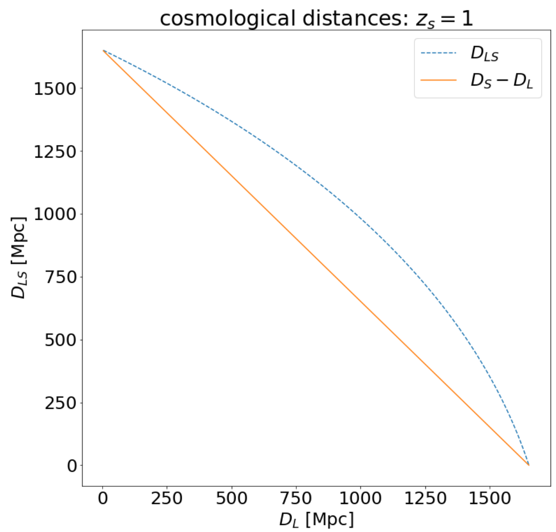

MICROLENSING OF MULTIPLY IMAGED QSOs

The optical depth in this case can be much higher than for stars in our galaxy, even one or greater, making it probably that the source is being microlensed at any given time.

$$\tau = \frac{\kappa_*}{1 - \kappa_{\rm macro}}$$

The nature of the caustics depends strongly on the density of stars.

$\kappa = 0.2$ $\kappa = 0.5$ $\kappa = 0.8$

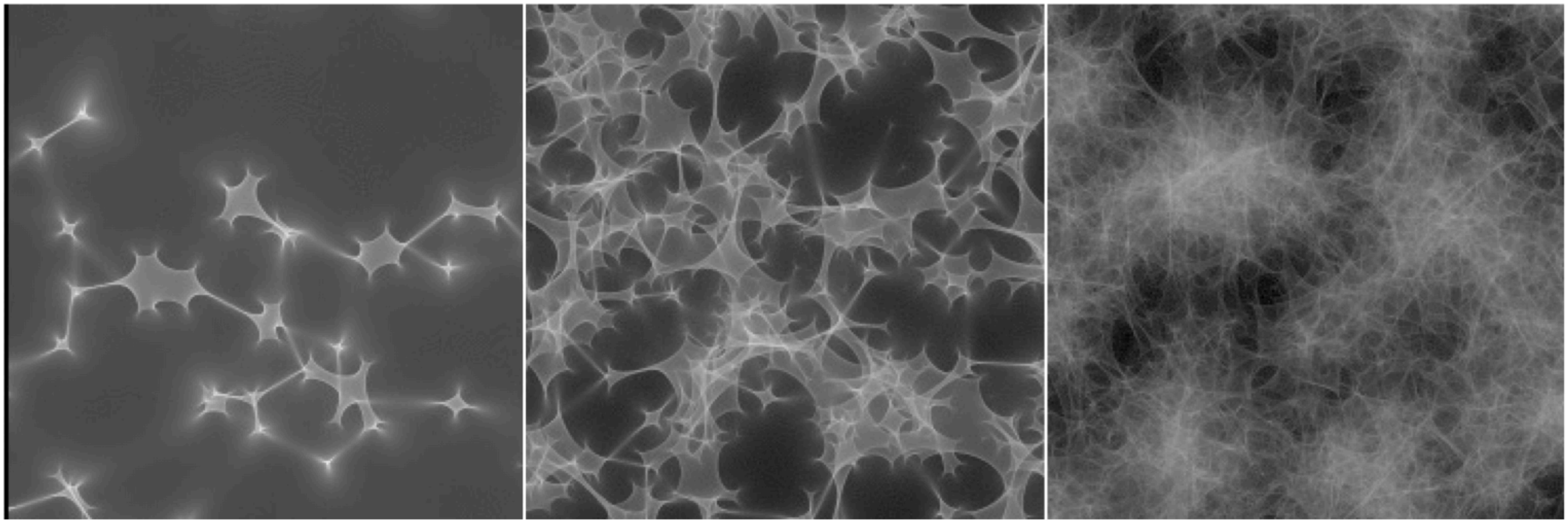

J. Wambsganss

MICROLENSING OF MULTIPLY IMAGED QSOs

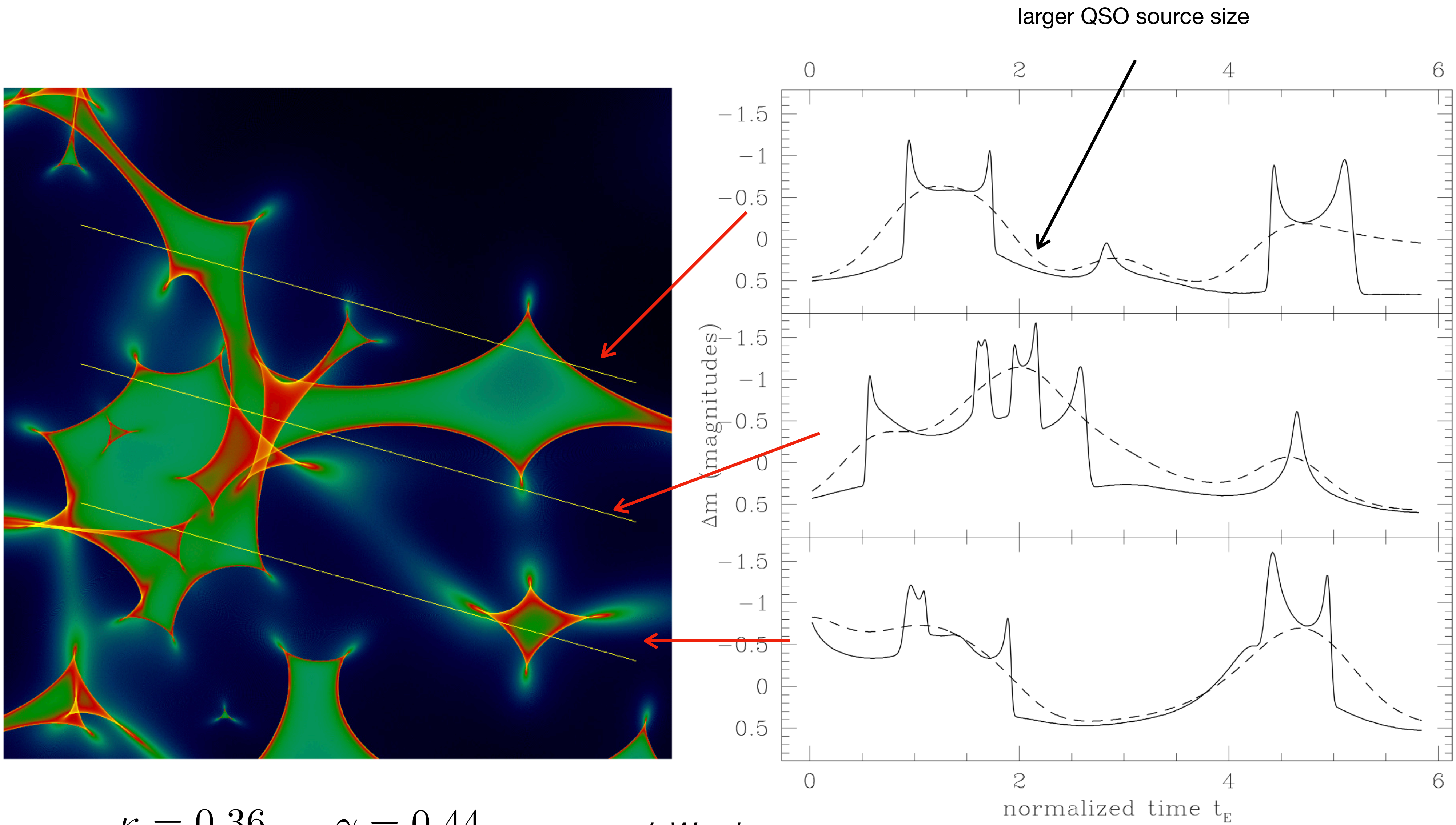

$\kappa = 0.36 \qquad \gamma = 0.44$

J. Wambsganss

MICROLENSING OF MULTIPLY IMAGED QSOs

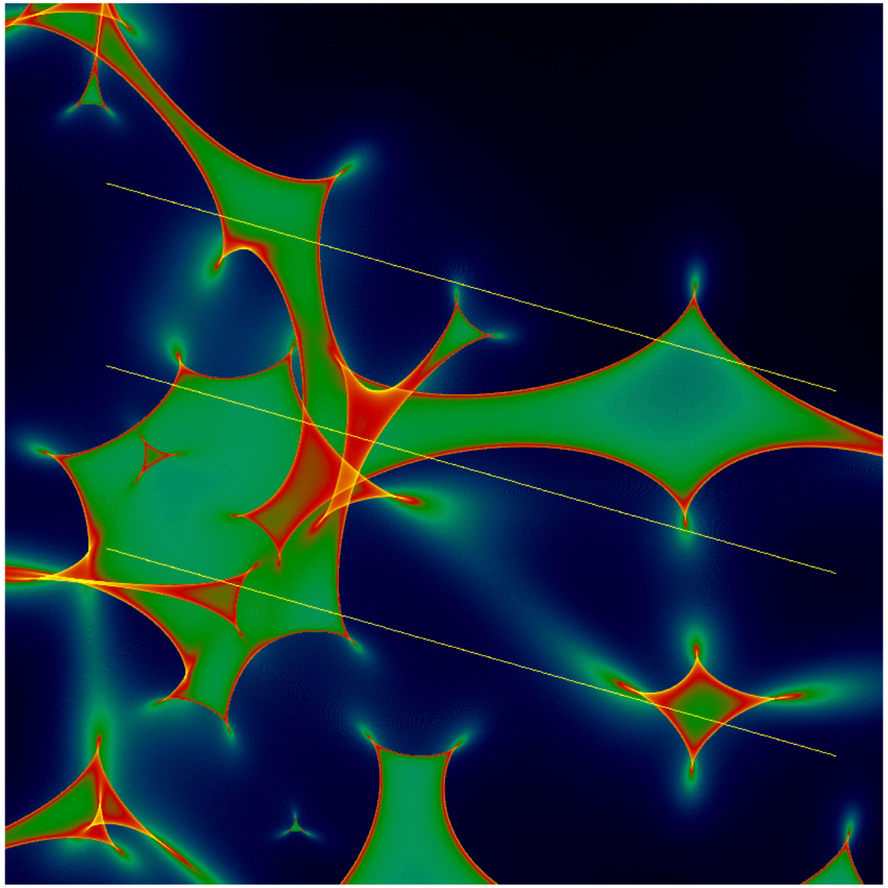

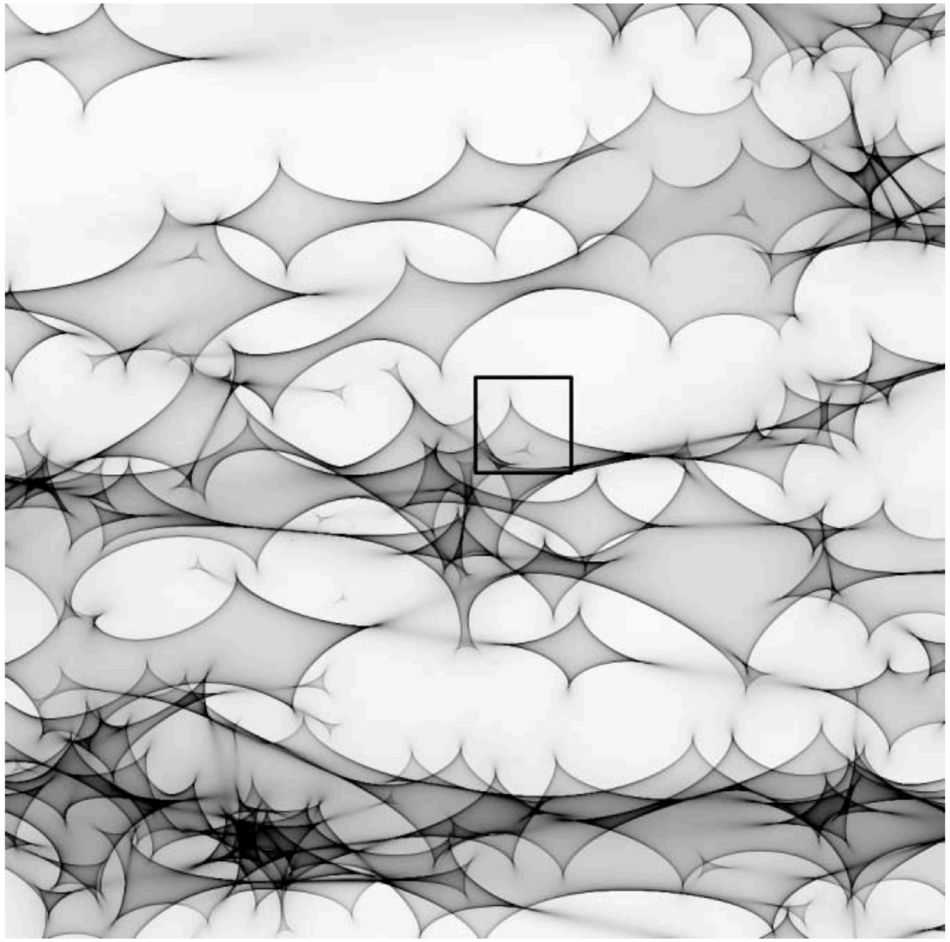

Microlensing map of QSO 2237+0305A image

MICROLENSING OF MULTIPLY IMAGED QSOs

micro-images of the accession disk of the quasar

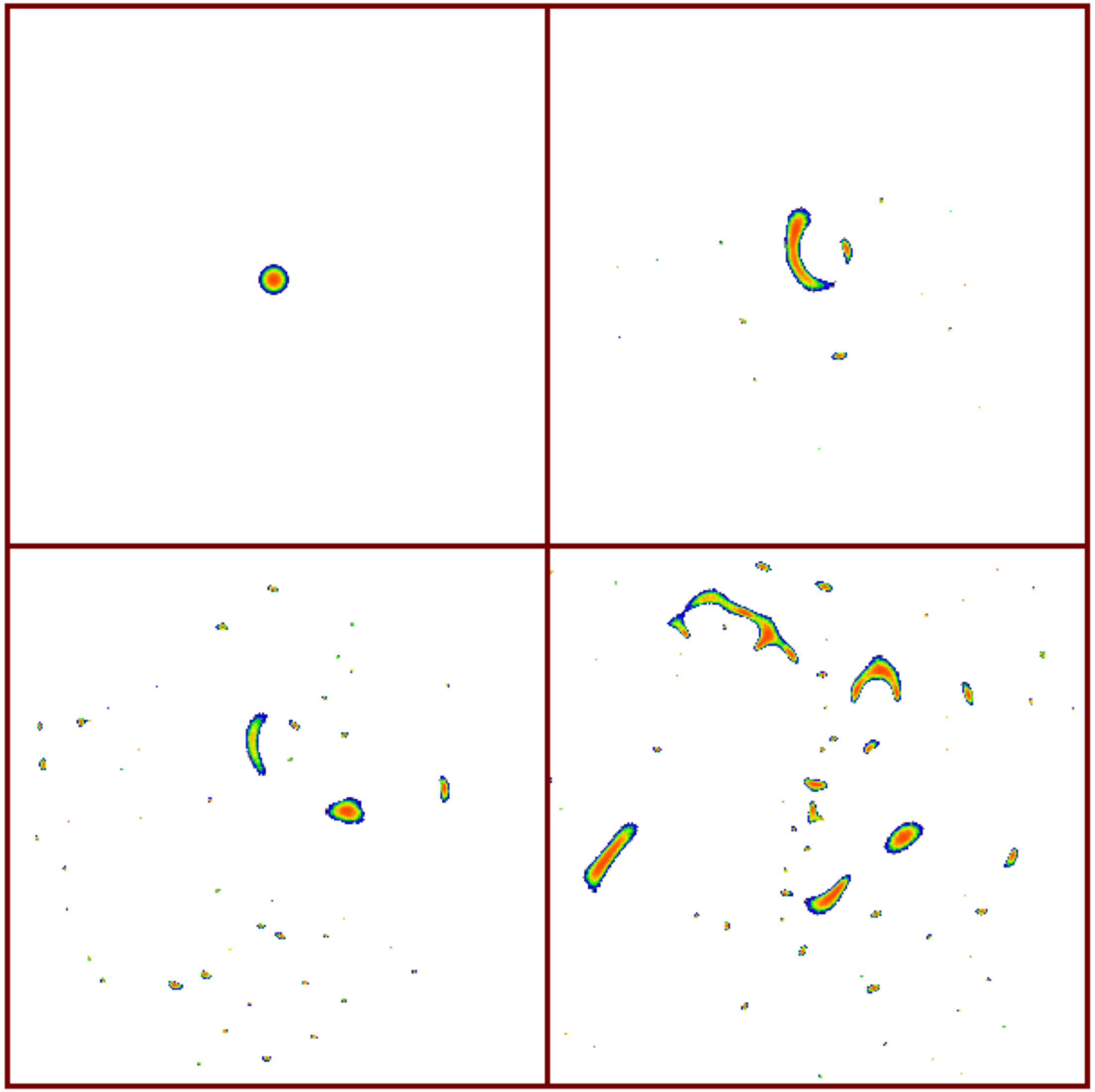

J. Wambsganss

MICROLENSING OF MULTIPLY IMAGED QSOs

Kundrić et al.

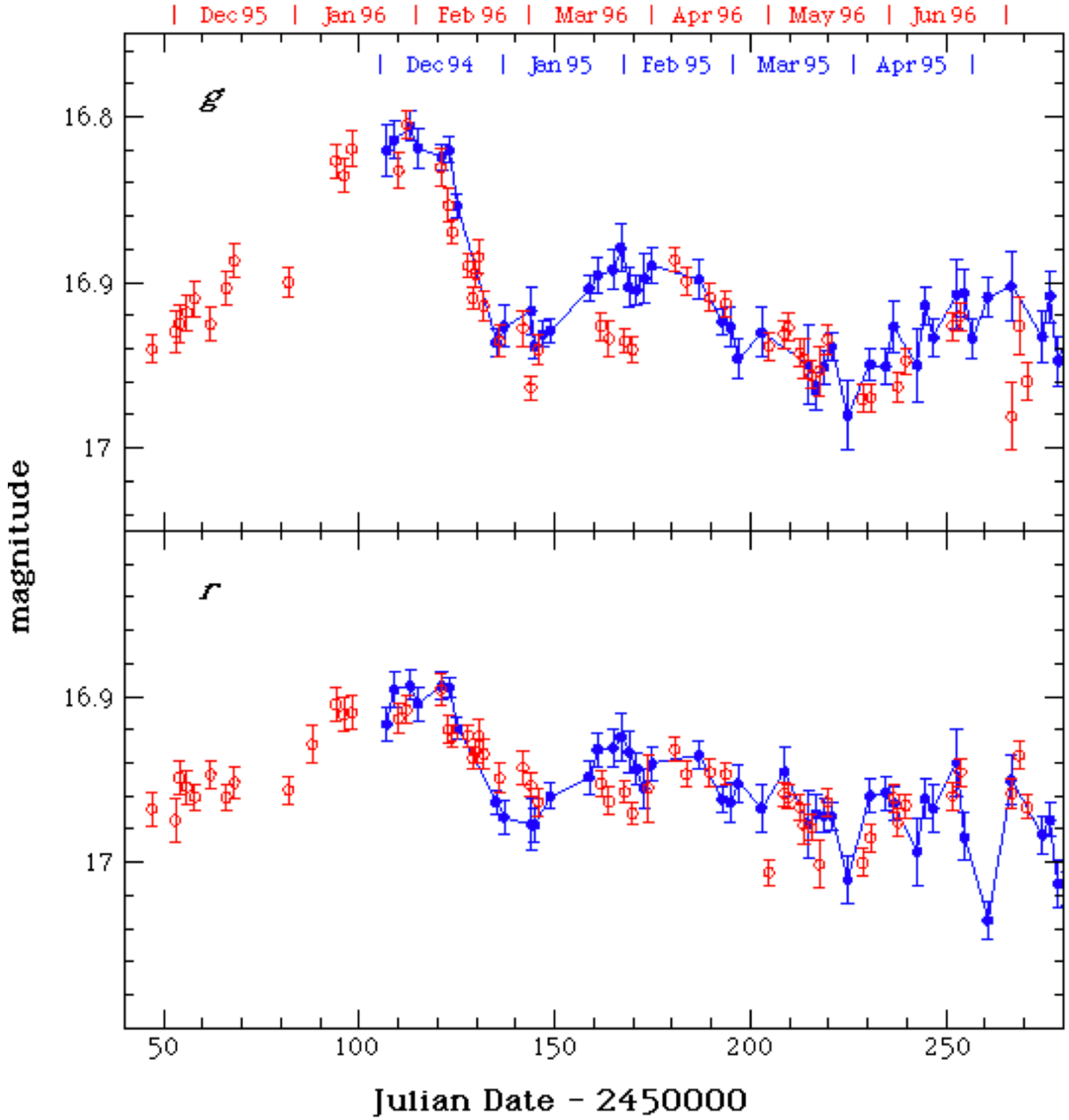

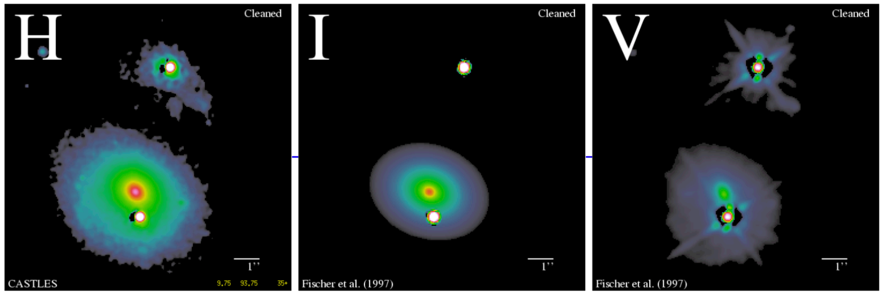

Q0957+561
images A (blue) and B (red)

First the time-delay must be measured.

Look for clear features in the light curves of different images that are repeated ofter a delay.

MICROLENSING OF MULTIPLY IMAGED QSOs

Kundrić et al.

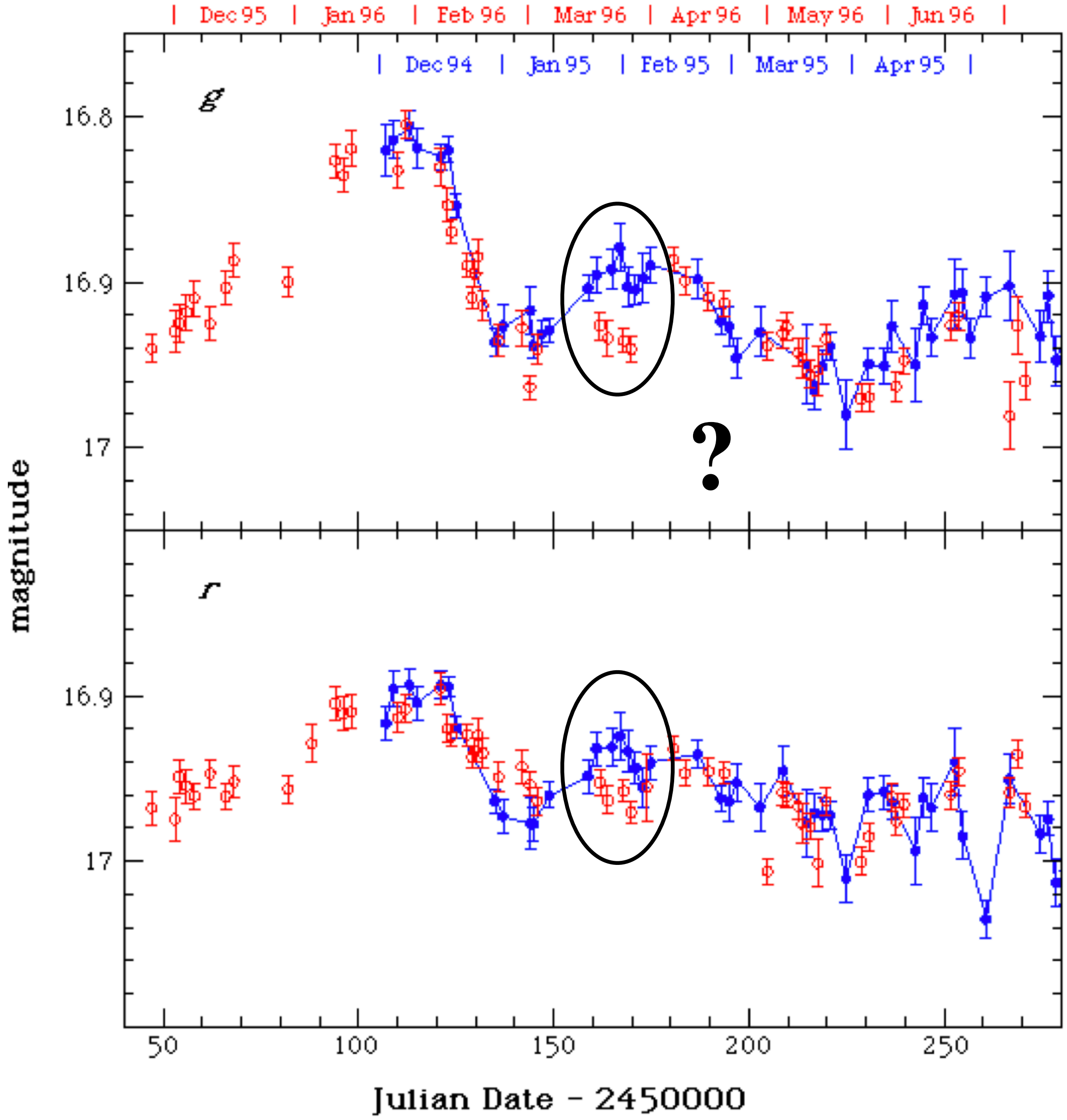

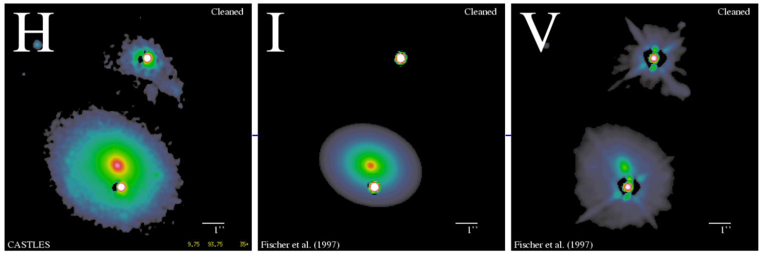

Q0957+561
images A (blue) and B (red)

First the time-delay must be measured.

Look for clear features in the light curves of different images that are repeated ofter a delay.

MICROLENSING OF MULTIPLY IMAGED QSOs

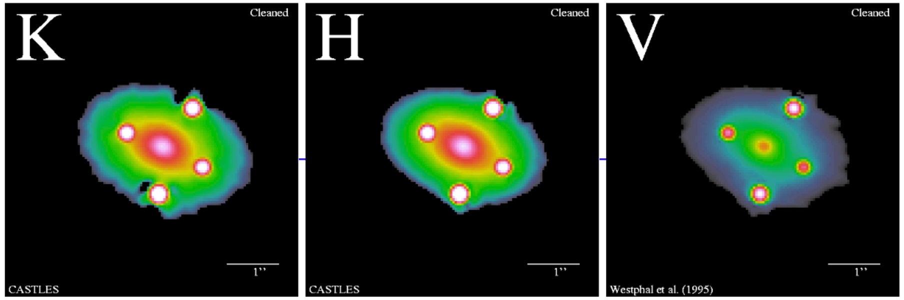

Example : 2237+0305

Particularly susceptible to micro lensing because the low lens redshift results in the images being close to the centre of the galaxy where the star density is high.

$$z_l = 0.04$$
$$z_s = 1.69$$

C image is clearly dimmer in 1991 then in 1994.

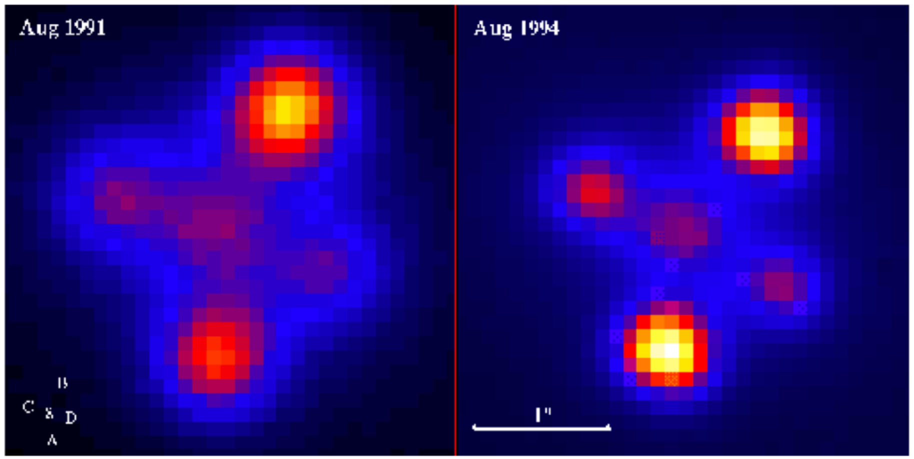

OGLE-II data

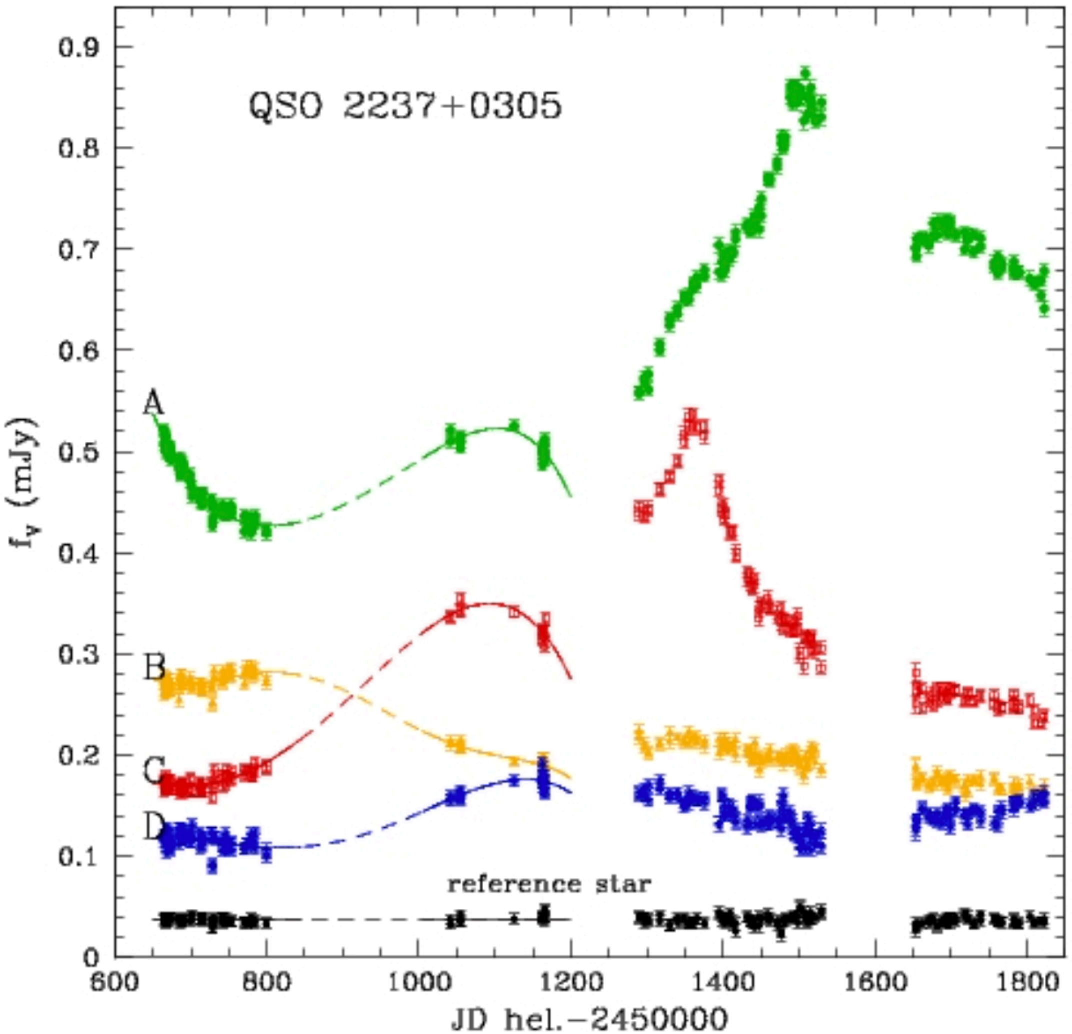

MICROLENSING OF MULTIPLY IMAGED QSOs

Spectroscopic microlensing

Classical model for the emission regions of a QSO

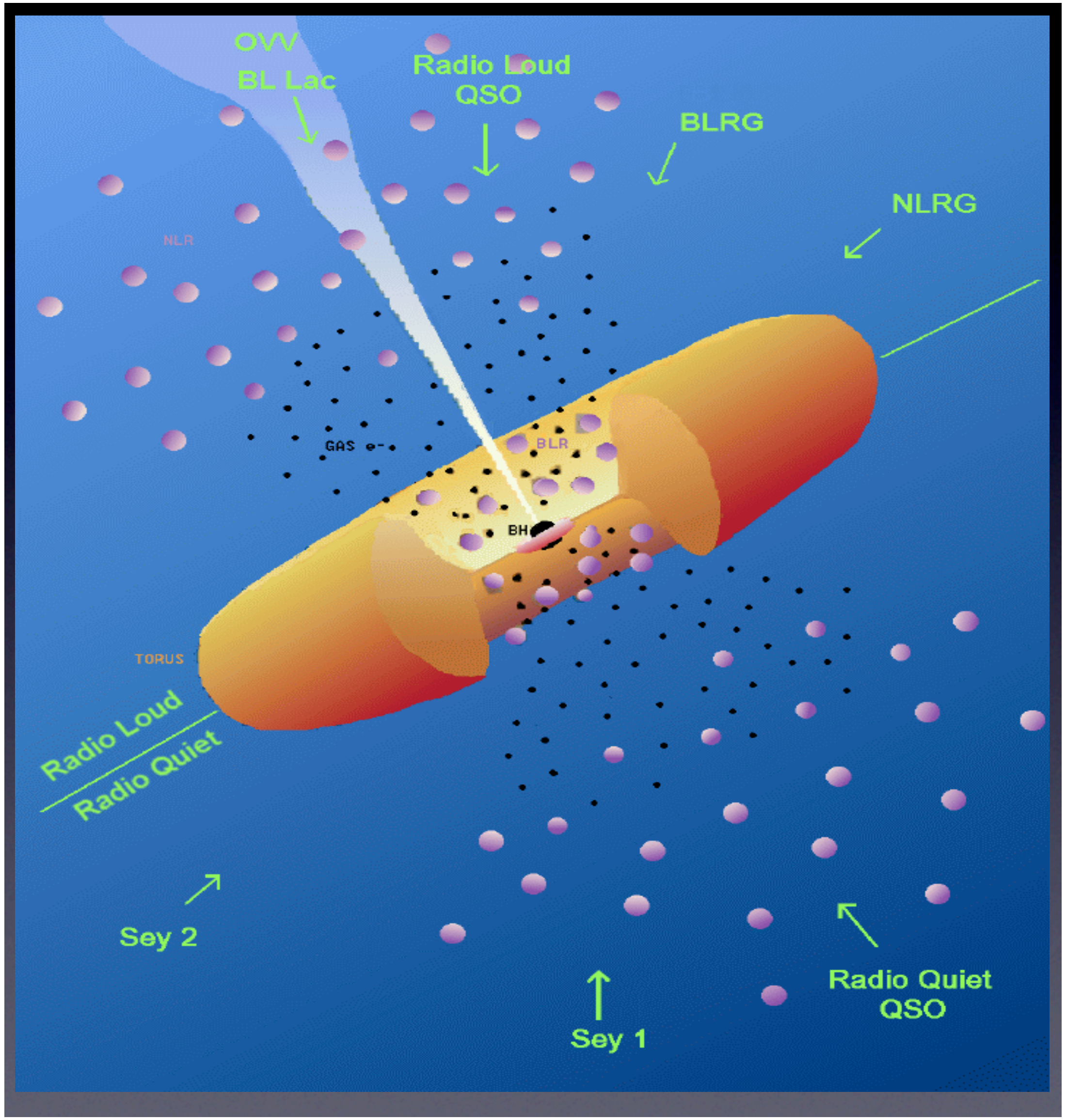

MICROLENSING OF MULTIPLY IMAGED QSOs

Spectroscopic microlensing

The different emission regions of a QSO produce emission lines in the spectra of each line.

Each emission region has a distribution of velocities causing the line profile.

Since the magnification is position dependent it will affect the line profile in a different way in each image that is micro lensed.

Hutsemékers et al. — Constraints on Quasar BLRs from Microlensing

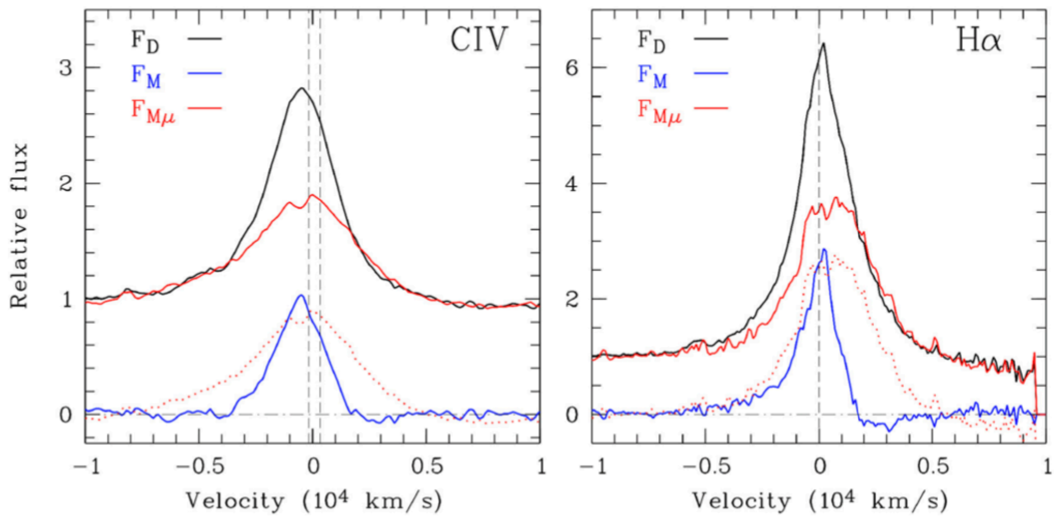

FIGURE 2 | Microlensing in the CIV and Hα lines of the quasar Q2237+030. F_D is the observed spectrum of image D which is not affected by microlensing. The line profile can be decomposed in a part affected by microlensing, $F_{M\mu}$, and another part not affected by microlensing, F_M, with $F_D = F_M + F_{M\mu}$. The dotted line profile represents the continuum-subtracted $F_{M\mu}$.

Here the emission line is decomposed into a microlensed part and an unlensed part.

MICROLENSING OF MULTIPLY IMAGED QSOs

Spectroscopic microlensing

The different emission regions of a QSO produce emission lines in the spectra of each line.

Each emission region has a distribution of velocities causing the line profile.

Since the magnification is position dependent it will affect the line profile in a different way in each image that is micro lensed.

Hutsemékers et al. Constraints on Quasar BLRs from Microlensing

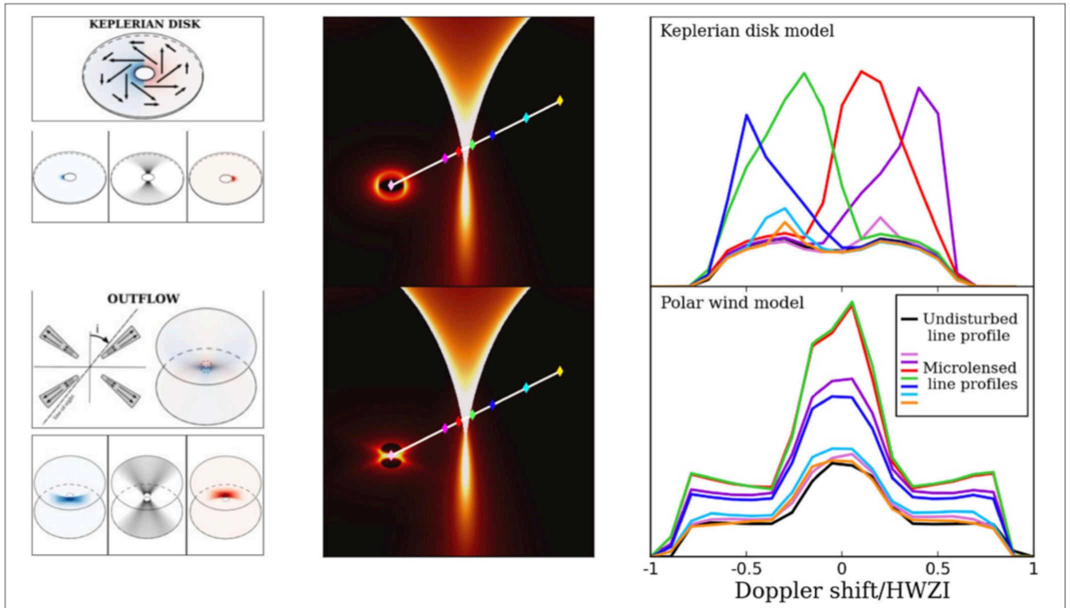

FIGURE 3 | Microlensing of different BELR structures and the resulting line profile distortions. The left panel sketches two models: a rotating Keplerian disk and a biconical outflow, both seen at intermediate inclination. The location of the approaching and receding gas is indicated in blue and red, respectively. The middle panel shows the BELR superimposed on a typical caustic. At the different positions indicated by colored losanges, different subregions of the BELR are magnified by the caustic. The right panel illustrates the line profiles corresponding to the different positions of the BELR onto the caustic pattern. Microlensing of the Keplerian disk is characterized by asymmetric red/blue line profile distortions while microlensing of the biconical outflow is characterized by symmetric wings/core distortions.

Different space-velocity distributions will result in different types of distortions got the lines.

An outflow will generally produce a symmetric distortion.

A orbital geometry will generally produce an asymmetric distortion.

QSO Microlensing

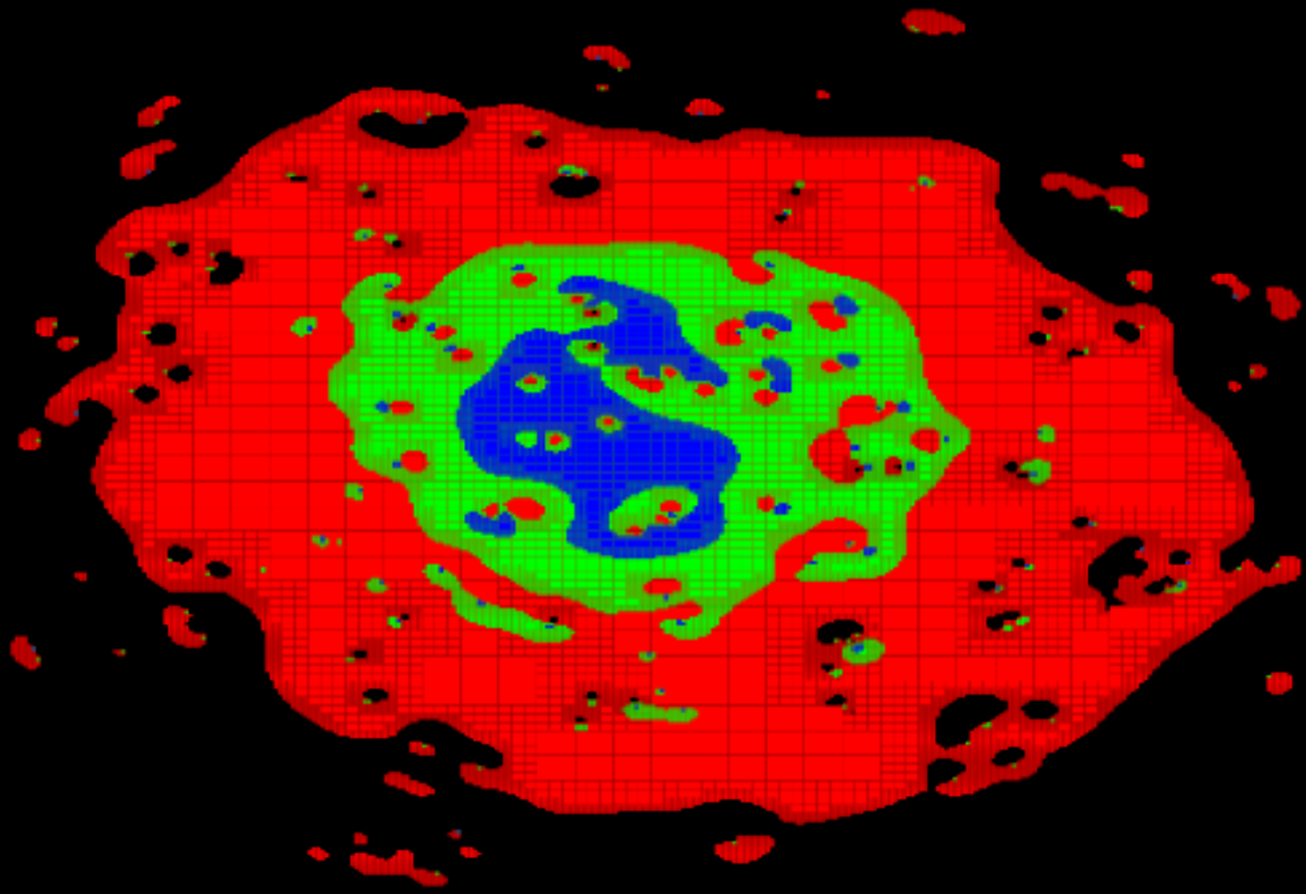

QSO Microlensing

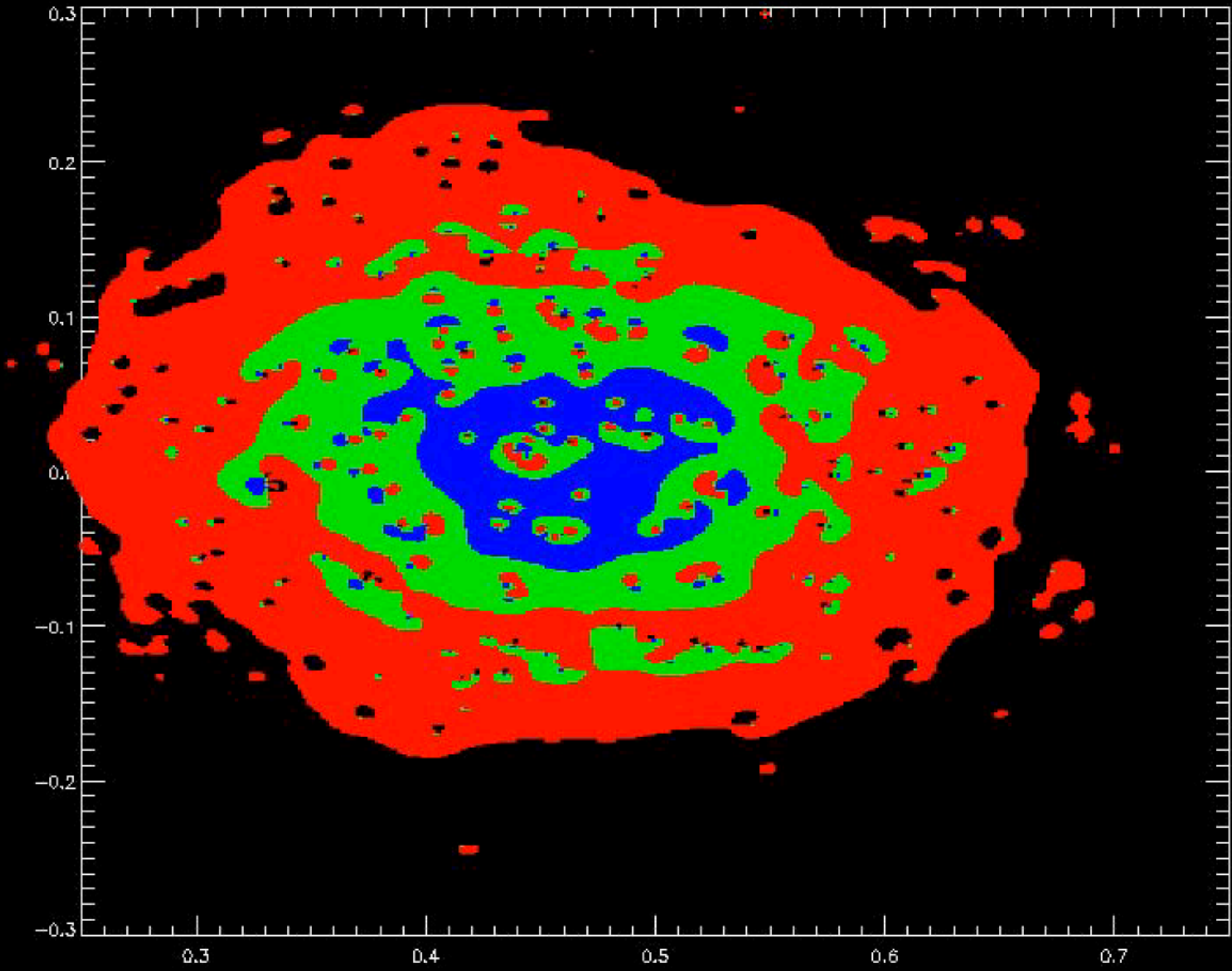

MICROLENSING OF MULTIPLY IMAGED QSOs

Lensing as a function of source size.